Polymer 50 (2009) 6100–6110

Contents lists available at ScienceDirect

Polymer

journal homepage: www.elsevier.com/locate/polymer

Correlation between processing parameters and microstructure of electrospun poly(*D*,L-lactic acid) nanofibers

Chi Wang [a,*], Huan-Sheng Chien [a], Kuo-Wei Yan [a], Chien-Lin Hung [a], Kan-Lin Hung [b], Shih-Jung Tsai [b], Hao-Jhe Jhang [c]

[a] *Department of Chemical Engineering, National Cheng Kung University, Tainan 701, Taiwan*
[b] *Industrial Technology Research Institute South, Nano-Powder & Thin Film Technology Center, Tainan 709, Taiwan*
[c] *Taiwan Textile Research Institute, No. 6, Chengtian Rd, Tucheng City, Taipei County 23674, Taiwan*

ARTICLE INFO

Article history:
Received 20 May 2009
Received in revised form
20 September 2009
Accepted 10 October 2009
Available online 30 October 2009

Keywords:
Electrospinning
PDLLA fibers
Microstructures

ABSTRACT

Using dimethyl formamide as the solvent, electrospinning of poly(*D*,L-lactic acid) (PDLLA, D-lactide content:10%) solutions with various concentrations was performed by means of a heating jacket for controlling the solution temperature range from 25 to 104 °C. In addition, an IR emitter was used to control the surrounding temperature at ~110 °C. The effects of solution properties and processing variables on the morphologies of the cone/jet/fiber were investigated, and the internal structure of the electrospun fibers was characterized using polarized FTIR, WAXD and DSC. A sufficient entanglement density existing in a given solution was an important requirement for successfully obtaining uniform fibers without beads. The log–log plot of specific viscosity (η_{sp}) versus PDLLA volume fraction (ϕ_v) provided us with a useful guideline to determine the entanglement concentration (c_e) for preparing fiber-shaped electrospun products. The ϕ_v-dependence of η_{sp} varied from $\eta_{sp} \sim \phi_v^{1.1}$ for a dilute solution to $\eta_{sp} \sim \phi_v^{4.7}$ for a solution possessing entangled chains. From the incipient concentration of entanglements, the determined c_e was ~10 wt%, which was in fair agreement with what was predicted theoretically by a simple relation of $2M_e/M_w$, where M_e and M_w were the molecular weight between melt entanglements and the average molecular weight of PDLLA, respectively. To obtain uniform PDLLA fibers without beads, however, a minimum concentration of $\sim 1.9c_e$ was required for the entangled solutions possessing sufficient network strength to prohibit the capillary instability during jet whipping. The log–log plots of the jet diameter (d_j) and fiber diameter (d_f) versus zero shear viscosity (η_o) showed two scaling laws existing for the present solution, that is, $d_j \sim \eta_o^{0.07}$ and $d_f \sim \eta_o^{0.45}$. For a given solution, an intimate relation between d_j and d_f was derived to be $d_f \sim d_j^{0.61}$, regardless of the variations of processing variables applied. High-temperature electrospinning produced small diameter fibers because of the reduction of η_o, but the effect was gradually diminished for solution temperatures higher than 56 °C owing to the enhanced solvent evaporation.

The as-spun nanofibers of this thermally slow-crystallizing PDLLA species were amorphous, and the Hermans orientation function calculated from the polarized FTIR results was ca. −0.063 regardless of the electrospinning conditions applied. This suggests that there was no preferential chain orientation developed in the nanofibers. In the heating in a DSC cell at a rate of 10 °C/min, however, rapid crystallization took place at 97 °C, followed by two well-separated melting endotherms centered at 121 and 148 °C, respectively. WAXD and FTIR results exhibited the exclusive presence of α-form crystals. These unique features were attributed to the occurrence of phase separation during electrospinning, which interrupted the chain orientation along the fiber during jet stretching, and yielded more trans–trans conformers with more extended chain structure to readily facilitate the cold crystallization during post-heating.

1. Introduction

Electrospinning is a powerful technique to produce polymer nanofibers with a diameter ranging from micro- to nanometer scale, depending upon the solution properties (viscosity, conductivity and surface tension) and processing variables (flow-rate,

* Corresponding author. Tel.: +886 6 2757575x62645; fax: +886 6 2344496.
E-mail address: chiwang@mail.ncku.edu.tw (C. Wang).

0032-3861/$ – see front matter © 2009 Elsevier Ltd. All rights reserved.
doi:10.1016/j.polymer.2009.10.025

applied voltage, and working distance) [1–4]. Melt electrospinning produces fat fibers due to the low conductivity and high viscosity of polymer melt in nature [5,6], whereas solution electrospinning yields thin fibers by carefully controlling the solution properties. Based on the previous reports, solution electrospinning is a preferred process to readily obtain fibers with a submicron diameter, and has been successfully applied to numerous polymers. It is well documented that viscosity is the most important solution property in determining the fiber diameter; the lower the solution viscosity, the thinner the fibers [7–10].

Poly(lactic acid) (PLA) has been widely used in various biomedical applications due to its biodegradability and biocompatibility. It is a degradable polymer derived from renewable sources and mainly used as an implant device, tissue scaffold, and internal suture [11–15]. By varying the relative ratio of *D*/L isomers along the backbone chains through chemical syntheses, either semi-crystalline or amorphous PLA can be obtained. Depending upon its microstructure developed in the processing as well as its hydrophobic nature, the degradation rate of PLA films can sometimes be slow, which can be a serious problem in a predominantly hydrophilic bio-environment. To increase the degradation rate of PLA, electrospinning is a promising technique in preparing fabrics towards the formation of controlled porous interior constituted by the electrospun nanofibers [15–22]. The fabric pore size is closely correlated with the fiber diameter. In contrast with the dense thin film, the fluid permeation and the specific surface area are increased in the PLA fabrics, both leading to a significant PLA degradation. On this basis, the manipulation of the fiber diameter of PLA through the electrospinning process becomes an important issue for controlling the subsequent degradation in its application as a tissue scaffold. Although PLA fibers could also be obtained from the melt-spinning process, the diameter of melt-spun fibers is rather large (50–200 μm) and the properties of PLA might deteriorate as a result of the thermal degradation at high temperatures required in the process. Recently, a novel melt electrospinning technique was reported using a CO_2 laser to melt the PLA pre-forms locally in an attempt to minimize thermal degradation [23]. Although fibers with a diameter of ~1 μm could be obtained, the laser melting induced molecular scission, which harmed the mechanical properties of the fibers. In the absence of thermal treatment, solution electrospinning seems inevitable to produce submicron PLA fibers to preserve the desired mechanical properties.

This work aims to provide a complete understanding of the effects of solution viscosity, flow-rate and applied voltage on the morphologies of cone/jet/fiber developed during electrospinning of the amorphous poly(*D*,L-lactic acid) (PDLLA) solutions. A designed heating apparatus was constructed for electrospinning at elevated temperatures. By varying the solution temperature, the chain entanglement status existing in the solution (which is the prerequisite condition for preparing uniform fibers) remained intact. However, the solution viscosity was reduced, giving rise to a feasible route to manipulate the as-spun fiber diameter. Our results presented a close relation between the solution rheology and the electrospun products, by which the minimum concentration for preparing uniform PDLLA fibers without beads could be predicted. Compared to the room-temperature electrospinning, the high-temperature process provided a feasible route for further diameter reduction. The microstructure of the as-spun fibers, characterized by several analytical techniques, showed a unique chain orientation of PDLLA, attributable to the liquid–liquid phase separation of the solution during the electrospinning process. A detailed study, starting with the properties of electrospinning solutions to the internal structure of the electrospun fibers, is presented.

2. Experimental

2.1. Solution preparation and properties

PDLLA pellets were obtained from Natureworks LLC. Dimethyl formamide (DMF) purchased from J.T. Baker (HPLC grade) was used as the solvent to prepare solutions with different PDLLA concentrations. Using a JASCO DIP-370 polarimeter at a wavelength of 589 nm, the specific optical rotation $[\alpha]_D^{25}$ of the PDLLA/chloroform solution with a concentration of 1 g/dL was −128.4 at 25 °C. This corresponded to a molar fraction of 0.10 for the D-lactide unit [14]. By using gel permeation chromatography with chloroform as the mobile phase, the measured weight average molecular weight (M_w) and polydispersity index of PDLLA were determined to be 1.78×10^5 g/mol and 2.1, respectively. The intrinsic viscosity [η] at 25 °C was 0.9825 dL/g and the Huggins constant was 0.379, measured using the capillary viscometer together with the Huggins equation. The reported solubility parameters for PDLLA, chloroform, and DMF are 10.6–11.4 [24], 9.3, and 12.1 $(cal/cm^3)^{0.5}$, respectively. Compared to the chloroform commonly used as a solvent for PLA, DMF is an acceptable solvent owing to its sufficiently high conductivity. The main drawbacks of using chloroform as the electrospinning solvent for PDLLA are the low conductivity and high volatility, which lead to a great difficulty in the process control. To prepare electrospinning solutions with different concentrations, weighted amounts of PDLLA and DMF were mixed and vigorously stirred for several hours. Prior to electrospinning, degassing was performed to remove the small bubbles in the solutions. Using the density values of 1.230 and 0.944 g/cm^3 for PDLLA and DMF, respectively, the conversion of weight fraction to volume fraction (ϕ_v) for the as-prepared solution can be carried out. Solution properties, such as surface tension (γ), conductivity (κ), and zero shear viscosity (η_o) were measured at various temperatures using the Face surface tension meter (CBVP-A3), Consort conductivity meter (C832), and Brookfield viscometer (LVDV-I+, spindle 18, and cup 13R), respectively. In addition, the linear viscoelastic properties of the solutions were measured in the ARES rheometer using the cup-and-bob feature at different temperatures. The oscillatory shear mode was applied to determine the storage shear modulus $G'(\omega)$ and loss shear modulus $G''(\omega)$ over a range of frequencies (ω). η_o was determined from the loss modulus data at low frequencies: $\eta_o = \lim_{\omega \to 0} G''(\omega)/\omega$, and the recoverable shear compliance J_s^o was determined from the storage modulus at low frequencies: $J_s^o = 1/\eta_o^2 \lim_{\omega \to 0} G'(\omega)/\omega^2$. The relaxation time τ_0 was then estimated by $\tau_0 = \eta_0 \cdot J_s^o$ [25]. The specific viscosity η_{sp} of the PDLLA solution was calculated as $(\eta_o - \eta_s)/\eta_s$, where η_s is the viscosity of DMF solvent (0.802 cP).

2.2. Processing and measurements

Fig. 1 shows the schematic diagram of the high-temperature electrospinning system. A jacket-type heating device was used to maintain the PDLLA solution at a desired temperature for electrospinning. Circulation of the heated silicone oil was fulfilled by a pumping system connected to an oil bath where the temperature could be adjusted to 140 °C. A significant temperature gradient was found along the needle owing to its "one-dimensional fin" geometry, giving rise to an apparent temperature difference for the solutions within the jacket tube and those within the electrified Taylor cone. To resolve this problem, an IR emitter was used for maintaining a sufficiently high environmental temperature to reduce the temperature difference. The temperature of the "Taylor cone" measured by a thermocouple was used to represent the solution temperature for electrospinning. When the system reached a thermal equilibrium, the as-prepared solution was delivered by

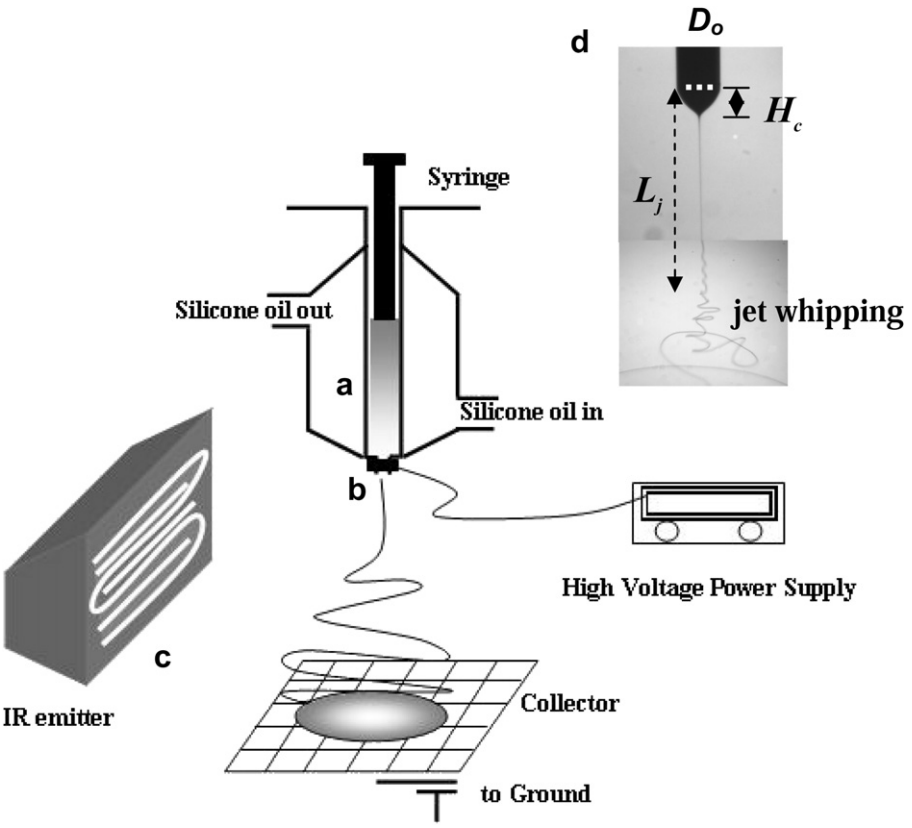

Fig. 1. Schematic apparatus for the high-temperature electrospinning process, (a) a jacket-type heat exchanger using a circulating oil as the heating medium to maintain the PDLLA/DMF solution at a desired temperature, (b) a needle used as the spinneret connected to a high-voltage source, (c) an IR emitter heating device for controlling the surrounding temperature, (d) the morphology of stable cone-jet electrospinning mode as observed by the present CCD setup. D_o is the outer diameter of needle, H_c is the cone height, L_j is the length from the needle end to the initial point of jet whipping.

a syringe pump (Cole–Parmer) at a controlled flow-rate (Q) ranging from 0.1 to 5 mL/h to the needle (D_i/D_o/length = 1.07/1.47/40.0 mm, unless otherwise indicated), where a high electrical voltage (V) ranging from 6 to 25 kV was applied by a high-voltage source (Bertan, 205B). To construct a needle-to-plate electrode configuration, a steel net ($30 \times 30\ cm^2$) was used as a collector for the electrospun fibers at a certain working distance (H) below the needle tip. Four CCDs were used to observe the morphologies of the electrified cone and jet during electrospinning, that is, (1) the cone height, H_c, defined by the distance from the needle end to the Taylor-cone apex, (2) the length of the straight jet, l_j, measured from the apex of the Taylor-cone to the initiation of jet whipping, (3) the terminal jet diameter at the end of straight jet, d_j, determined by a laser diffraction technique, and (4) the jet whipping behavior observed by a high-speed camera (Redlake, Motion Pro 10000) to capture the images at a rate of 10^4 frames/s. The length from the needle end to the initial jet whipping was denoted as $L_j\cdot(=H_c + l_j)$. The experimental details are described in a previous article [26]. For the needle-to-plate electrode configuration, the electric field calculation was performed using the FLUX2D9.10 software to solve the 3-D electrostatics problem [27]. The relative permittivity of air was set at 1.0 and ca. 6000 triangle elements were used to solve the Poisson equation. The electric field intensity was derived by the gradient of the calculated potential, and the intensity at the initial whipping position ($z = L_j$) was then determined and denoted to be E_j.

2.3. Fiber characterization

The morphology of the fibers was observed under a scanning electron microscope (SEM, Hitachi S4100). The fiber diameters were measured from a collection of ~500 fibers, from which the average fiber diameter (d_f) was determined. Thermograms were obtained by using a differential scanning calorimeter (Perkin Elmer Co., DSC7) under a nitrogen atmosphere at a scanning rate of 10 °C/min. Crystallinity values were determined using the ratio of $\Delta H_f/\Delta H_f^o$, where ΔH_f and ΔH_f^o are the measured DSC heat of fusion and the heat of fusion for a 100% PLA crystal. A value of $\Delta H_f^o = 93.1$ J/g [11] was used to calculate the degree of crystallinity. The IR polarization measurements were made using the FTIR spectrometer (Perkin Elmer Co., Spectrum 100) equipped with a polarizer. Two successive IR measurements with parallel and perpendicular polarization of the electric vector with respect to the aligned fiber direction were performed. Aligned PDLLA fibers were collected between two grounded sharp blades separated by a distance of 10 mm. To monitor the changes in chain orientation as a consequence of processing variations, the $\nu(C=O)$ absorption band of the spun PDLLA fibers was evaluated to calculate the Hermans orientation function. Dichroic ratio (R) was calculated using the formula $R = A_{//}/A_{\perp}$, where $A_{//}$ and $A_{\perp}$ are the absorbances with the polarized IR beam, parallel and perpendicular to the fiber direction, respectively. A rotating-anode X-ray generator (Rigaku Co., Dmax2000) with mono-chromatized Cu K_α beam was used to obtain the wide-angle X-ray diffraction (WAXD) intensity profile of the samples. The porosity of fiber membranes was calculated from the density measurement according to the procedure suggested by Zong et al. [28]. Mechanical properties of the fiber membranes were obtained from the stress-strain curve using a universal tensile testing machine (Instron 4500) at a stretching rate of 10 mm/min. Specimens with dog-bone shape were prepared using a sharp cuter. The mean thickness of each sample was ~35 μm. The gauge length and

sample width were 15 and 4 mm respectively. The reported data of mechanical properties represent the average results of three tests.

3. Results and discussion

Because water is a non-solvent for PLA [24], the presence of moisture in the vicinity of the needle will affect the development of a stable Taylor cone. Sometimes a severe cone blockage takes place if the humidity is too high. To resolve this problem, a gas jacket was used to introduce sufficient N_2 to appropriately encapsulate the Taylor cone without interrupting the jet bending during electrospinning [26].

3.1. Entanglement concentration (c_e)

Electrospun products with a fiber-like structure can only be obtained under the condition that a chain network is developed in the given electrospinning solution. For solutions with a concentration lower than c_e, electrospinning is eventually degenerated to electrospraying, which yields spherical particulates because of the capillary instability at the end of the straight jet. Thus, for a given polymer/solvent pair the determination of c_e is an important task prior to electrospinning. On the basis of the method proposed by McKee et al. [7], the log–log plot of the solution's specific viscosity (η_{sp}) versus volume fraction (ϕ_v) was constructed (Fig. 2) to determine the c_e for the present PDLLA/DMF solutions. The rapid viscosity increase at ~8 vol.% (10 wt.%) suggested the existence of a chain entanglement occurring around this concentration, where the final linear domain is first seen. It indicates the transition from the unentangled to the entangled solution regime. For the entangled solution with a concentration higher than c_e, all data fall on the straight line with a constant slope of 4.68. In contrast, an exponent of 1.15 is derived for the dilute solution regime, which is consistent with the theoretical prediction. The overlapping concentration c^* was estimated by $\sim 1/[\eta]$ to be 0.82 vol.%, leading to the c_e/c^* ratio of ~9.8. As seen in Fig. 2, a significant slope change takes place for a concentration variation from c^* to c_e. Theoretically, c_e can also be estimated by the classical relation $c_e = 2M_e/M_w$, where M_e is the molecular weight between entanglements in the melt state. After substituting the values of $M_w = 1.78 \times 10^5$ and $M_e = 5600$ g/mol [see Appendix], the calculated value of c_e is ~6.3 vol.%, which is in fair agreement with the experimentally determined one.

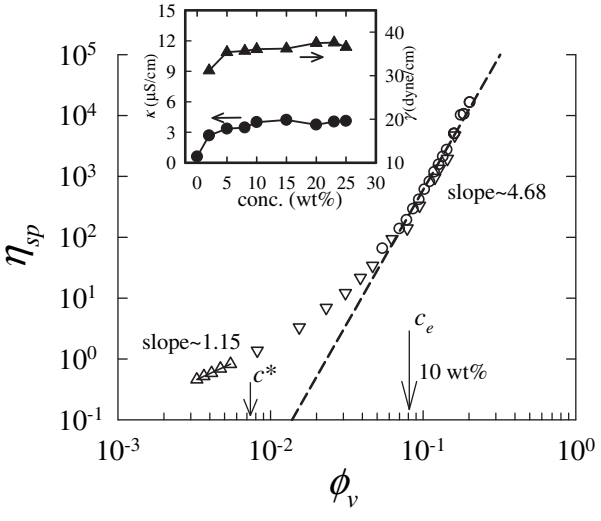

Fig. 2. A plot of specific viscosity, η_{sp}, versus volume fraction of PDLLA, φ_v, at ambient temperature. Open circles are obtained from ARES rheometer, open inverted triangles from Brookfield viscometer and open triangles from capillary viscometer. The deviation of the final straight line is starting at a concentration of 10 wt%, from which the chain entanglement concentration, c_e, is determined. The inset shows the concentration dependence of solution conductivity, κ (filled circles), and surface tension, γ (filled triangles).

Our dynamic viscoelastic results also provided the solution concentration dependence of J_s^o and τ_o and two scaling laws were derived: $J_s^o \sim \phi_v^{-1.71}$ and $\tau_o \sim \phi_v^{2.7}$. It is of interest to note that the relaxation time is in the range of several ms, which is in a comparable order with the time scale for electrospinning; τ_o increased from 0.4 ms for the 9 vol.% solution to 1.7 ms for the 13 vol.% solution. Also displayed in Fig. 2 (inset) are the measured κ and γ values of solutions with different concentrations. As the PDLLA concentration is increased, κ gradually increases and finally reaches a plateau value of ~4.0 μS/cm in the entangled solution regime. A similar trend is observed for the γ with a plateau value of ~37.0 dyne/cm. Because both κ and γ remain unchanged in the entangled regime, the present PDLLA/DMF solution can serve as a model solution for the concentration variations to exclusively disclose the viscosity effect on the cone/jet/fiber morphologies developed during the electrospinning process.

Fig. 3 shows the obtained products from the electrospinning process of the PDLLA solutions with different concentrations. Consistent with the prediction by the solution rheological data, a fiber-like structure is first seen in the solutions with a concentration of 8–10 wt.%, below which only spherical particulates are collected. In order to obtain the bead-free fibers, however, a minimum concentration of ~19 wt.% is needed. This suggests that not only the presence of chain entanglement but also a sufficient entanglement density is required to develop a deformable network for preventing the network rupture during electrospinning. Our results are in agreement with previous studies that showed that the solution concentration should be as large as 1.8–2.5 c_e in order to yield uniform fibers [7,8]. To reveal the concentration effect on the fiber diameter, solutions with a concentration of 19–25 wt.% were electrospun to exclude the consideration of beaded fibers for a fair comparison. On the other hand, a solution with a concentration higher than 25 wt.% was too viscous to be electrospun, and an inhomogeneous status was observed due to the solubility limitation. Prior to electrospinning, the functioning domain was constructed in order to select the common *V and Q* to apply [27]. Due to the low volatility of the DMF solvent, a relatively high working distance of 28 cm was used to obtain the solvent-free fibers, which was validated by the absence of the DMF characteristic absorbance in the FTIR spectra. For a given *Q*, a small range of *V* is available for the desired cone-jet electrospinning mode. By increasing *Q*, *V* is increased and a wider range of *V* becomes available. Moreover, a larger *V* is generally required for a more concentrated solution. A common but limited processing window does exist and the determined *Q* and *V* are 1 mL/h and 12.5 kV for electrospinning the entangled solutions.

Applying the same processing variables (*H*, *Q* and *V*), the measured H_c, L_j, and d_j all increased with increasing η_o (Table 1). For the present needle-to-plate configuration setup, the electric field strength is highly non-uniform and concentrated around the needle end [26]. Since E_j decays exponentially with the distance from the needle end, a larger L_j eventually leads to a lower E_j for jet whipping. It has been pointed out that the jet diameter, as well as how effectively the jet whipping takes place are relevant to the final fiber diameter [27]. In other words, two stages of jet stretching are considered during electrospinning. Due to the excess surface charge at the Taylor cone surface, the first jet stretching initially takes place at the cone apex to the straight jet end, which proceeds to whipping. The level of jet diameter reduction was estimated by D_o/d_j to be ~210. Further jet stretching takes place in the whipping region and the amount of diameter reduction, estimated by the

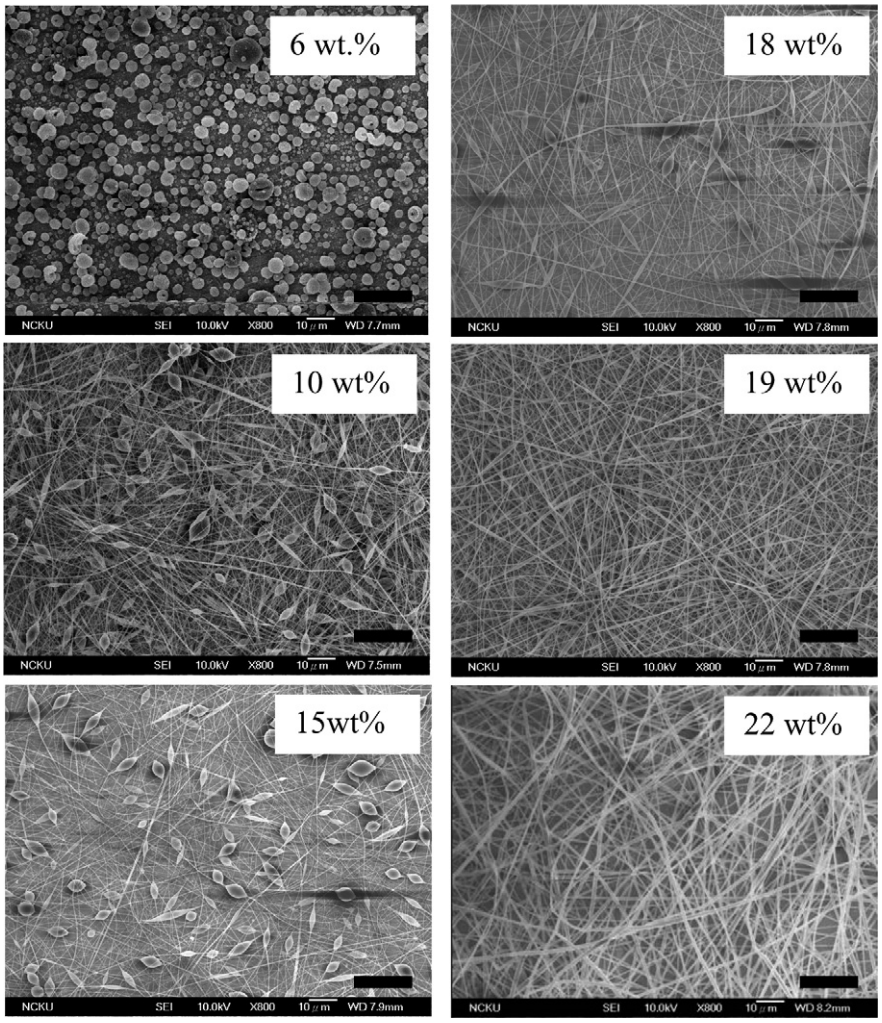

Fig. 3. SEM images of electrospun products obtained from different PDLLA concentrations. The scale bar is 20 μm [$H = 28$ cm, $Q = 1.0$ mL/h, 7.0–12.5 kV].

ratio of d_j/d_f, was found to be ~10 for the solutions studied. It should be noted that significant solvent evaporation also occurs during jet whipping, leading to the gradual increase of the PDLLA concentration and the final solidification. It is evident that the initial jet stretching associated with the repulsive forces at the cone surface is the dominant stage in determining the fiber diameter. Although manipulation of the jet whipping process is not feasible due to its "bending instability" behavior, a more effective whipping is expected provided that E_j is higher. In short, a straight jet with a smaller d_j together with a shorter L_j is desirable to produce electrospun fibers with a smaller d_f. Table 1 also displays the jet velocity $v_j (= 4Q/\pi d_j^2$, by assuming negligible solvent evaporation) at the straight jet end as well as the jet drawability $[=(d_j/d_f)^2\phi_v]$ during whipping. It is interesting to note that despite the high value of v_j (~8 m/s), the straight jet showed the tendency to undergo "electric bending" due to the overcrowded surface charges and the small surface perturbation. The drawability is decreased with the increasing solution viscosity, indicating a less effective jet whipping. The dichroic ratio of the carbonyl absorption band remained unchanged as the solution viscosity was increased from 3522 to 12,910 cP, suggesting the intactness of the main chain orientation developed in the as-spun fibers, as discussed in the later part. Compared to the more conductive polyacrylonitrile (PAN)/DMF solutions [26], however, the present PDLLA/DMF solution exhibits a higher drawability. Fig. 4 shows the double logarithmic plots of d_j and d_f versus η_o, from which two scaling laws are derived as $d_j \sim \eta_o^{0.07}$ and $d_f \sim \eta_o^{0.45}$. In addition, the corresponding plots for the PAN/DMF solutions reported previously [26] are included. PAN solutions possess a higher conductivity (35–51 μS/cm) than the PDLLA solutions. However, in terms of surface tension, the values are similar (PAN solution's value is ~36.3 dyne/cm). It is intriguing to note that similar exponents are derived from the two different solutions; d_j is found to be relatively independent of the viscosity, whereas an exponent of ~0.45–0.52 is observed for the viscosity dependence of d_f. Our derived exponents for the η_o dependence of d_f are in fair agreement with the polyhydroxybutyrate solution (~0.36–0.41) [27] but are evidently lower than those of the polyester solution (~0.80) [7] and polymethyl methacrylate solution (~0.72) [29].

Table 1
Solution viscosity effect on the morphologies of cone/jet/fiber as well as the dichroic ratio of PDLLA fibers.

wt (%)	η_0 (cP)	H_c/D_0	L_j/D_0	E_j (kV/m)	d_j (μm)	d_f (nm)	Drawability	v_j (m/s)	R
20	3522	0.99	4.2	295.0	6.39 ± 0.31	419 ± 105	36.9	8.7	1.55
22	5664	1.04	4.5	270.3	6.45 ± 0.22	522 ± 118	26.8	8.5	1.55
23	8296	1.11	5.1	230.6	6.63 ± 0.13	611 ± 141	21.7	8.0	1.55
25	12910	1.38	7.3	146.2	6.93 ± 0.43	723 ± 189	18.5	7.4	1.52

$Q = 1$ mL/h, $H = 28$ cm, 12.5 kV.

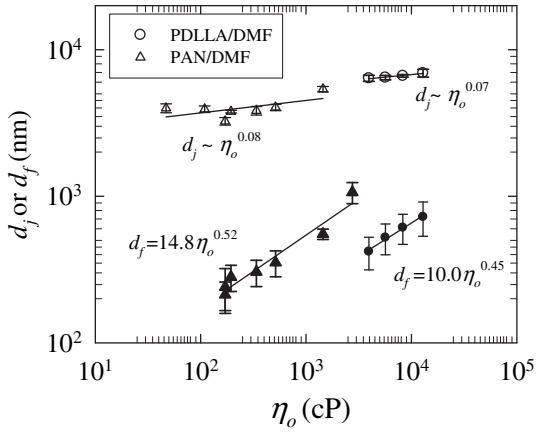

Fig. 4. Viscosity effect on the jet diameter (open symbols) and fiber diameter (filled symbols) for the PDLLA/DMF solutions as well as the PAN/DMF solutions. [The processing variables for the PDLLA solutions are $H = 28$ cm, $Q = 1$ mL/h, and 12.5 kV, whereas $H = 7$ cm, $Q = 0.3$ mL/h, and 6 kV are used for the PAN solutions [26]].

Using both solutions at a fixed η_o, the electrospinning of the PAN solutions produces a thicker fiber than the PDLLA counterpart. The nominal electric field, V/H, calculated for the PAN and PDLLA solutions are 85.7 and 44.6 kV/m, respectively. Based on the first principle, electrospun PAN fibers would have a smaller diameter due to its possession of a lower d_j (Fig. 4) together with a higher V/H for jet whipping. Based on the finite element calculation, however, it was remarked that the electric field distribution was not uniform, indicating that it was inappropriate to use the V/H ratio to represent the electric field. Moreover, the magnitude of the electric field was found to be proportional to the applied V, and independent of H in the jet whipping region [27]. Thus, the pronounced diameter reduction of PDLLA fibers is eventually attributed to the application of a high voltage (12.5 kV) which, in turn, gives rise to the high E_j for jet whipping (Table 1). For the more conductive PAN solution, a low voltage of 6.0 kV was sufficient to develop a stable electrospinning mode, leading to a low E_j of 180 kV/m for jet whipping. On the other hand, when the applied voltage was higher than 8 kV, unstable electrospinning of the PAN solution was seen with multiple straight jets issuing from the cone apex [26], that is, a condition outside the functioning domain of processing. Due to the possession of a larger E_j, the electrified PDLLA jet eventually experiences a more significant jet stretching during whipping than the PAN jet, as revealed by a pronounced increase of drawability from ~9 for the PAN to ~30 for the PDLLA jet.

According to Figs. 2 and 4, on the basis of the solid content a simple relation is expressed by $d_f \sim \phi_v^{2.11}$ for electrospinning the PDLLA solution. Being consistent with previous PLA findings [16,18], our results showed that the diameter of PDLLA fibers increases with increasing solution viscosity (or PDLLA concentration). Moreover, it has been pointed out that further diameter reduction of the electrospun PLA fibers could be achieved by adding ionic salts or using conductive co-solvent to enhance the solution conductivity [16,18].

3.2. Effects of processing variables (H, Q and V)

Although H shows a negligible influence on the diameter of the electrospun fibers [9], a minimum H is generally required for solvent evaporation to prepare solvent-free fibers. To study the Q and V effects on the electrospinning of the 22 wt.% PDLLA solution, H is fixed at 28 cm for this purpose. Table 2 shows the effects of processing variables on the morphologies of the Taylor cone, straight jet and electrospun fibers as well the fiber dichroic ratio. For a fixed Q, as the applied voltage is increased, H_c is decreased but L_j is relatively unchanged. The calculated E_j is slightly increased by increasing V. In spite of the limited range of voltage available, the jet diameter evidently decreases from 11.7 μm at 13.5 kV to 7.9 μm at 16.5 kV. The observed trends for both d_j and E_j support the experimental finding that a thinner PDLLA fiber is obtained when a higher V is applied. With the increase in V, the jet velocity is increased, although the drawability is decreased.

In contrast with the limited range of V, a broader processing window for Q is available for the electrospinning process (Table 2). As the flow-rate is increased under a constant V of 15.5 kV, the Taylor cone becomes bigger, and a longer and thicker jet is evidently obtained. The Q-dependence of d_j exhibits a power law relation and is expressed by $d_j \sim Q^{0.61}$. Similar exponents were also derived for the polystyrene solutions in different solvents (~0.44–0.66) [9] and the polyhydroxybutyrate solution (~0.61) [27]. With the increase of Q from 1 to 4 mL/h, the calculated E_j is apparently reduced from 268 to157 kV/m, suggesting that a less effective whipping occurs for the thicker jet and thus fibers with a larger diameter are expected (Table 2). For the present PDLLA/DMF solutions, Q is found to be the most important processing variable, instead of H and V, to manipulate the free jet diameter as well as the fiber diameter. A similar conclusion has been reported for the PS solutions [9]. When a higher Q is applied, in contrast with the V effect, the jet velocity is decreased but the drawability is increased. Moreover, the main chain orientation remained relatively unchanged, judging from the constant value of R (Table 2) in spite of different processing variables applied.

In summary, for a given solution the diameter of the electrospun fiber is mainly dependent upon two measured quantities, that is, d_j and E_j. In other words, a straight jet with a smaller d_j and shorter length will experience an enhanced E_j for a more effective whipping process, leading to the production of fibers with a lower d_f. Based on the above arguments, an intimate relation between d_j and d_f should exist and may provide a guideline for manipulating the electrified jet to prepare as-spun fibers with a desired diameter. Much efforts have been devoted to predicting the final fiber diameter by solving the complicated equations involving the fluid dynamics as well as the electrostatics [30–33]. Due to the coupled

Table 2
Effects of applied voltage and flow-rate on the morphologies of cone/jet/fiber as well as the dichroic ratio of PDLLA fibers.

Voltage (kV)	Q (mL/h)	H_c/D_0	L_j/D_0	E_j (kV/m)	d_j (μm)	d_f (nm)	drawability	v_j (m/s)	R
13.5	2	1.50	6.0	203.2	11.66 ± 0.40	797 ± 196	37.6	5.2	1.42
14.5	2	1.29	6.1	215.1	10.29 ± 0.31	758 ± 163	32.4	6.7	1.42
15.5	2	1.04	6.0	233.3	9.56 ± 0.37	680 ± 140	34.7	7.7	1.39
16.5	2	0.72	6.3	234.7	7.94 ± 0.11	591 ± 142	31.7	11.2	1.38
15.5	1	0.59	5.4	267.5	5.86 ± 0.26	498 ± 115	24.3	10.3	1.37
15.5	2	1.04	6.0	233.3	9.56 ± 0.37	680 ± 155	34.7	7.7	1.39
15.5	3	1.40	7.7	169.8	11.41 ± 0.28	731 ± 191	42.8	8.2	1.40
15.5	4	1.71	8.2	157.3	13.76 ± 0.50	804 ± 171	51.4	7.5	1.38

22 wt% solution, $H = 28$ cm.

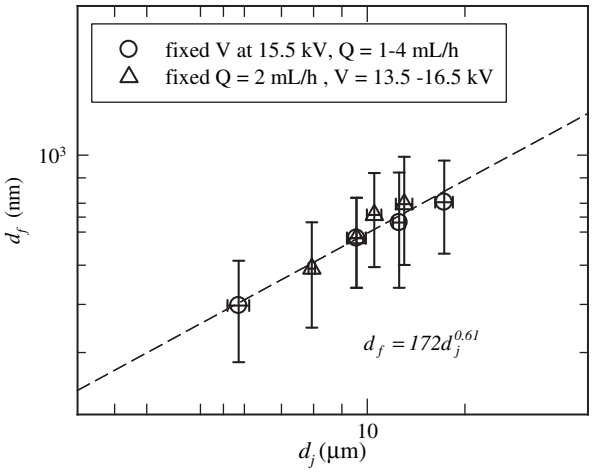

Fig. 5. A plot of fiber diameter versus jet diameter obtained from electrospinning of the 22 wt.% solution by changing the flow-rate (circles) and applied voltage (triangles), respectively. [$H = 28$ cm].

effects of solvent evaporation and "bending instability behavior" [31], the theoretical derivation of the d_j–d_f relation becomes rather difficult, if not impossible. By constructing the log–log plot of measured quantities, the relation between d_j and d_f is experimentally revealed as shown in Fig. 5. For a given electrospinning solution, it is worth noting that all the measured data are superimposed to form a master curve by an expression of $d_f \sim d_j^{0.61}$, regardless of the processing variables. Similar exponents have also been obtained for the polystyrene solutions ($\sim$0.45) [9] and the polyhydroxybutyrate solutions ($\sim$0.54) [27]. Without consideration of the jet stretching during jet whipping, a simple relation for the d_j–d_f relation is intuitively derived and readily used: $d_f = \phi_v^{0.5} d_j^{1.0}$ [31,33]. Our derived exponent indicated that jet stretching associated with the whipping process should not be neglected in determining the final d_f and the strength of jet stretching could be estimated by the calculated drawability.

3.3. High-temperature electrospinning

As mentioned previously, the prerequisite condition for preparing uniform fibers is the presence of sufficient entanglement density in the electrospinning solution. By varying the solution temperature, the chain entanglement status existing in the solution remains intact, but solution viscosity is significantly altered, giving rise to a feasible route for manipulating the as-spun fiber diameter. To reveal the temperature effect on the solution properties, shear experiments on the 20 wt.% PDLLA solution were carried out at several elevated temperatures; the solution viscosity was pronouncedly decreased from 3522 to 273 cP when the temperature was raised from 25 to 94 °C. Assuming that the temperature dependence of η_o was governed by the Arrhenius-type equation, a flow activation energy (ΔE_η) of 33.9 kJ/mol was obtained. Similarly, κ and γ of the polymer solutions at various temperatures were measured. With the increase of the solution temperature from 25 to 85 °C, κ was slightly increased from 6.5 to 7.9 μS/cm and γ was slightly decreased from 36.1 to 33.8 dyne/cm. All these trends favored the production of thinner fibers at elevated temperatures. The corresponding activation energies, that is, ΔE_κ and ΔE_γ, were derived to be 0.36 and 0.12 kJ/mol, respectively, indicating a weak temperature dependence of κ and γ. Thus, for a given solution, η_o can be adjusted by tuning the operating temperature to a different level in an attempt to produce thin PDLLA fibers. Using the 20 wt.% PDLLA solution, electrospinning was performed at various solution temperatures under a processing condition of $Q = 1$ mL/h, $H = 14$ cm, and 12.5 kV. The surrounding temperature was kept constant at 110 °C by means of the IR emitter. To prevent a high temperature gradient along the needle length, a short needle with a small diameter (D_i/D_o/length = 0.69/1.07/4.0 mm) was used as the spinneret. Table 3 shows the results of the solution temperature effect on the cone/jet/fiber morphology as well as the chain orientation. As the temperature of the electrospinning solution is increased from 25 °C to 68 °C, a bigger cone accompanying a shorter and thinner straight jet is observed, and a higher E_j is derived for an enhanced jet whipping. These findings imply that d_f would be reduced with increasing solution temperature. A slight increase of solution temperature to 37 °C leads to a pronounced reduction of d_f. However, the effect becomes less distinct for temperatures higher than 56 °C. The marginal effect on the d_f reduction is attributed to the enhanced solvent evaporation at high temperatures, which may readily increase the jet viscosity and retard the effective jet whipping. When solution temperature was higher than 68 °C, solvent evaporation was very significant that cone blockage took place, giving rise to an unstable electrospinning mode.

3.4. Internal structure of PDLLA fibers

Fig. 6 shows the typical FTIR spectra for the carbonyl group (1800–1720 cm^{-1}) with the polarized IR (a) parallel to and (b) perpendicular to the fiber axis for revealing the chain orientation developed in the PDLLA fibers. Since the as-spun fibers were amorphous as revealed by WAXD (Fig. 9), the orientation of the carbonyl group was used to determine the main chain orientation. Two important features deserve to be noticed. The first is the significant shift of the absorbance peak from 1752.0 cm^{-1} for parallel IR to 1761.5 cm^{-1} for the perpendicular IR transmission, and the second is the observation that the measured $A_{//}$is greater than $A_\perp$, giving rise to a dichroic ratio larger than unity. As mentioned previously, the dichroic ratio of the carbonyl group of the as-spun fibers is always greater than unity regardless of various processing conditions applied (Tables 1–3). This is rather unexpected in view of the fact that its transition moment vector is almost perpendicular to the main chain. In addition, provided that the PDLLA chains preferably orient to the fiber axis direction, the value of R should be lower than 1.0. Four conformers with different helical structures, that is, *tt* 2_1, *gt* 10_3, *tg* 5_1, and *gg* 4_1, are reported for the PLA polymers and their corresponding IR absorbance peaks are 1749.1, 1759.0, 1767.3, and 1776.2 cm^{-1}[34], respectively. It should be noted that the C = O groups orient perpendicularly to the helix axis for the *gt*, *tg*, and *tt* conformers, but are in parallel to the helix axis for the *gg* conformer. The difference in the helical conformation further indicates that the *gg* conformer exhibits the least chain expansion, whereas the *tt* conformer possesses a more

Table 3
Solution temperature effect on the morphologies of cone/jet/fiber as well as the dichroic ratio of PDLLA fibers.

Temp. (°C)	η_o (cP)	H_c/D_0	L_j/D_0	E_j (kV/m)	d_j (μm)	d_f (nm)	R
25	3522	0.84	11.2	102.4	4.09 ± 0.11	503 ± 118	1.38
37	1971	1.12	10.5	112.0	3.48 ± 0.14	352 ± 102	1.34
45	1267	1.21	11.2	102.4	3.57 ± 0.09	318 ± 85	1.50
56	789	1.31	8.8	148.0	3.43 ± 0.11	308 ± 79	1.42
68	588	1.59	8.6	153.3	2.91 ± 0.17	309 ± 61	1.42
87[a]	337					329 ± 78	
104[a]	201					324 ± 85	

20 wt% solution, surrounding temperature of 110 °C, short needle (D_i/D_o/length = 0.69/1.07/4.0 mm).
[a] Unstable electrospinning mode.

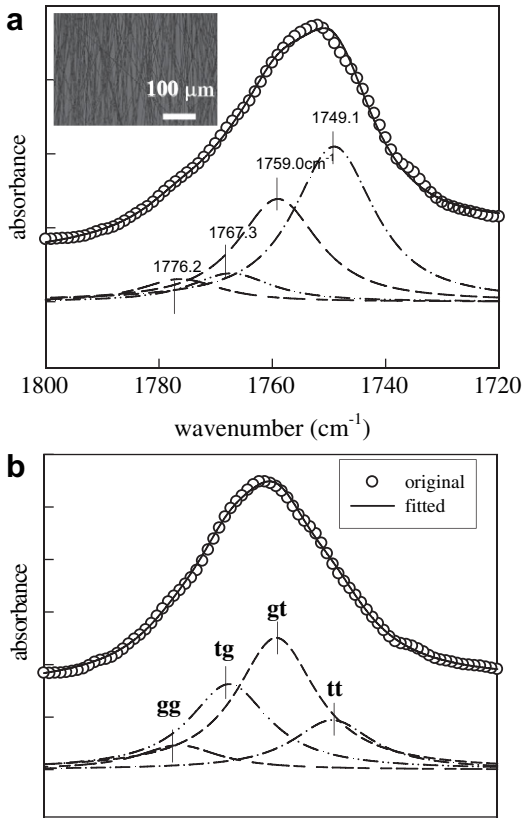

Fig. 6. FTIR spectra of aligned PDLLA fibers with the polarized IR (a) parallel to the fiber axis, (b) perpendicular to the fiber axis. The open symbols are measured data and the solid line is the resultant curve of the four curves (dashed lines) obtained from the de-convolution of the original spectrum. The corresponding absorbance peaks for *tt*, *gt*, *tg* and *gg* conformers are 1749.1, 1759.0, 1767.3 and 1776.2 cm^{-1}, respectively. The inset shows the OM image of aligned fibers collected for analysis.

extended chain character. By de-convolution of the polarized IR spectra (Fig. 6), the volume fraction of each conform can be estimated and the results are shown in Fig. 7 which also shows the IR-angle dependence. The anisotropy of the molecular chains is apparently exhibited since the *tt* content in the fiber direction is higher. However, the content gradually decreases with the increasing azimuthal angle, which is compensated for by the relative content of the *tg* conformer. On the other hand, the variation of both *gt* and *gg* conformers is rather mild. Thus, the shift of the

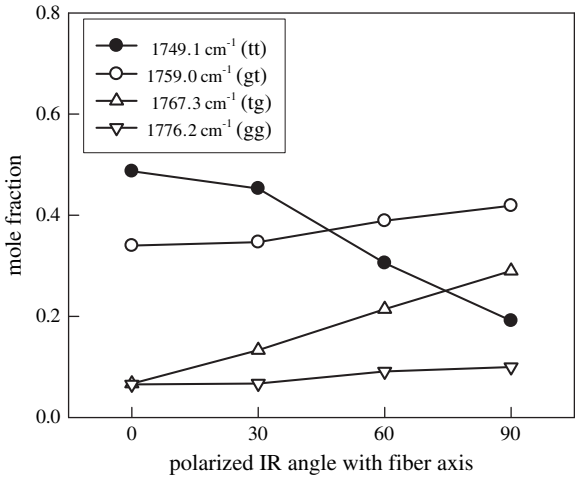

Fig. 7. Azimuthal angle dependence of PDLLA conformer concentration.

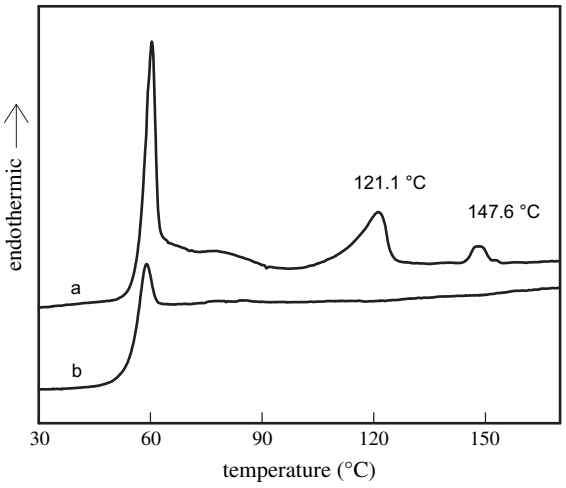

Fig. 8. DSC heating trace of the as-spun fibers (curve a) prepared by room-temperature electrospinning of a 22 wt% solution operated at: $H = 14$ cm, 1 mL/h, and 11.5 kV. After the first heating at a rate of 10 °C/min to 190 °C, the sample is cooled at 10 °C/min to 10 °C, and the second heating run is subsequently performed (curve b).

global absorbance peak as shown in Fig. 6 is attributed the content variation of the *tt* and *tg* conformers. For the electrospun PDLLA fibers, the content of the *tt* conformer (~0.35) is higher than that reported for the cast film, ~0.28 [34], suggesting that a more dense packing of PDLLA chains is developed in the fibers. To determine the chain orientation, the Hermans orientation function (f) related to the second moment of molecular orientation $< \cos^2 \theta >$ can be correlated with the measured dichroic ratio, and can be expressed as [35]

$$f = \left[3 < \cos^2\theta > -1\right]/2 = [(R_o + 2)/(R_o - 1)][(R - 1)/(R + 2)] \quad (1)$$

where $R_o = 2\cot^2 \psi$ with ψ being the angle between the transition moment vector and the chain axis. Depending upon the main chain orientation, the value of f is between −0.5 and 1.0. The lower limit value represents the chain alignment in the plane perpendicular to the fiber direction, whereas the upper limit is for the PDLLA chains orienting perfectly parallel to the fiber axis. The value $f = 0$ corresponds to the random chain orientation in the fiber.

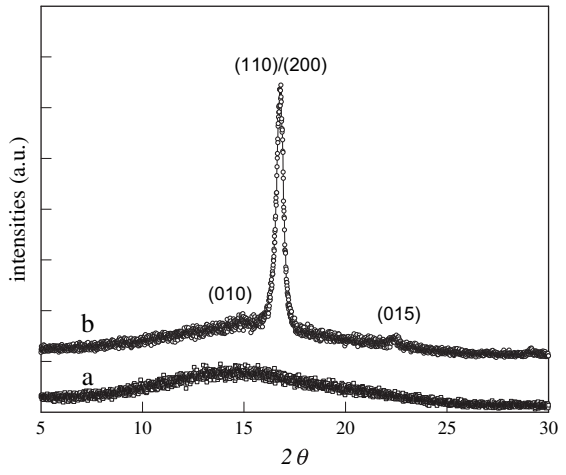

Fig. 9. WAXD intensity profiles of (a) as-spun PDLLA fibers (b) PDLLA fibers after annealing at 91 °C for 5 min [electrospinning of 20 wt% solutions at room temperature, $H = 14$ cm, 1 mL/h, 11.5 kV].

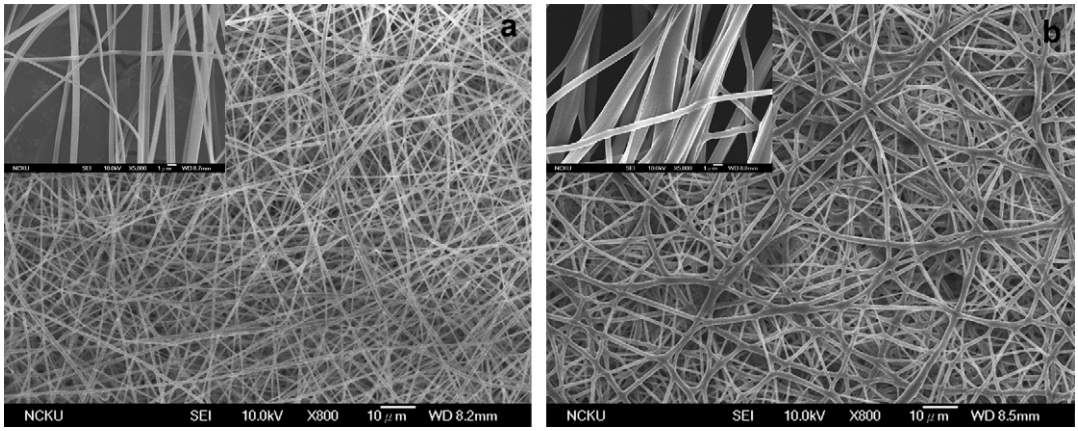

Fig. 10. SEM images of fiber morphologies (a) prior to, (b) post to the isothermal annealing at 91 °C for 5 min. The insets show a higher magnification.

For the carbonyl groups, ψ can be assumed to be 90°. Since the measured R is greater than 1.0 under all the processing conditions in the present system, the main chains prefer to align perpendicularly to the fiber direction, giving rise to the inapplicability of Equation (1). A similar situation has been reported in the determination of the orientation of the poly[(R)-3-hydroxybutyrate] chains in its blends with cellulose acetate butyrate [35]. To resolve this difficulty, the orientation of C = O itself (f_v) with respect to the fiber axis is determined to be $(R\text{-}1)/(R+2)$ by substituting $\psi = 0$ into Equation (1). Assuming that the main chain is distributed with cylindrical symmetry in the plane transverse to the C = O bond, a simple relation between f and f_v is derived to be [35]:

$$f_v + 2f = 0 \tag{2}$$

Regardless of the processing conditions used, the measured R of the as-spun fibers was between 1.34 and 1.55 (Tables 1–3), corresponding to the f_v value of 0.102–0.155. Based on Equation (2), the orientation function of the main chains was ca. −0.063. The negative small value of f suggested that no distinctive and preferred chain orientations were developed in the electrospun PDLLA fibers although significant jet stretching took place during the process. This is remarkably in contrast with the melt-spinning process, wherein significant chain alignment is induced along the fiber axis by the mechanical drawing [36].

The DSC heating scan of the as-spun PDLLA fibers at a rate of 10 °C/min is shown in Fig. 8 (curve a). The first heating run is characterized by a stepwise increase of specific heat at the glass transition of PDLLA at 55.9 °C, followed by a distinctive enthalpy recovery peak. This suggests that the free volume of PDLLA chains in the as-spun fibers is significantly reduced due to the possession of more *tt* conformers. The loss of enthalpy (ca. 4.0 J/g) associated with the free volume reduction will be recovered as the endothermic (aging) peak in the glass transition region. Another striking observation is the appearance of cold crystallization peak at 96.8 °C, followed by two melting peaks at 121.1 and 147.6 °C, respectively. After cooling the sample at a rate of 10 °C/min, the second heating trace shows a small enthalpy recovery of 0.6 J/g in the absence of crystallization and melting events (curve b). The observed T_g for the as-received PDLLA pellets, prior to electrospinning was 57.4 °C. While no T_m was detected (a thermogram similar to curve b) after 24 h annealing at 91 °C, our slow-crystallizing species finally developed a small crystallinity percentage of 6.5% with a single melting peak at 117.4 °C (not shown for brevity). Thus, electrospun fibers have provided a fast crystallization route, possibly due to the enhancement of the *tt* conformer. In other words, when annealing temperature is higher than the T_g of the membranes, the expansion of 2_1 helix of the *tt* conformer to 10_3 helix of the *gt* conformer (crystalline phase) is readily fulfilled paving the way for fast crystallization. The as-spun membranes are amorphous according to its WAXD intensity profile shown in Fig. 9, where the amorphous halo is the only one observed. Likewise, as given in Fig. 9, the intensity profile of membranes after being annealed isothermally at 91 °C for 5 min produced a discernibly pronounced diffraction peak at 16.5° together with two small peaks at 14.9° and 22.2°. These diffraction peaks are associated with the pseudo-orthorhombic α-form crystal with a 10_3 helical chain conformation [37]. The corresponding plane index is clearly presented. The confirmation of crystal modification was also verified by the FTIR spectrum (data not shown), in which the α-crystal-related band centered at 923 cm^{-1} was observed. In contrast, the band relevant with the β crystals at 912 cm^{-1} was not detected [38]. By the area ratio of the diffraction peaks to the total diffraction curve, the crystallinity percentage of the annealed membranes was determined to be 11%, which was consistent with that (∼10%) obtained by DSC. At this point, two important issues are left to be properly addressed. These are: the origin of the double melting peak of the as-spun amorphous PDLLA fibers as shown in Fig. 8 and the almost random distribution of the chain orientation in the electrospun fibers.

When crystallized, the PLA exhibits two possible crystal modifications (α and β forms) depending upon the crystallization condition. Because only the α-form crystal is detected according to the WAXD profile, the double melting behavior is not attributed to the polymorphism nature of the PLA. In addition, the possibility of the event of melting/re-crystallization/re-melting during the DSC heating scan is also ruled out because there is no trace of crystallization exotherm between these well-separated melting peaks (Fig. 8). We speculate that phase separation takes place during the electrospinning process to render the intriguing morphologies conserved in the as-spun PDLLA fibers. As a matter of fact, DMF is not a good solvent for the semi-crystalline PLLA, but can dissolve the amorphous PDLLA to some extent. Due to its relatively good conductivity, DMF is frequently used as a solvent in most of the electrospinning solutions. For a given electrospinning solution with a marginal miscibility, caution should be taken for the potential path from the miscible state to cross the binodal curve to reach the phase separation region. In other words, phase separation might take place during fiber formation through two plausible paths. The first is the significant solvent evaporation, especially in the jet whipping region, at a constant temperature, leading to an increase of polymer concentration in the whipping jet. The second is associated with the "evaporation cooling" effect of the electrospinning jet [39], resulting in the temperature drop of jet surface. The temperature reduction of the jet further provides a convenient

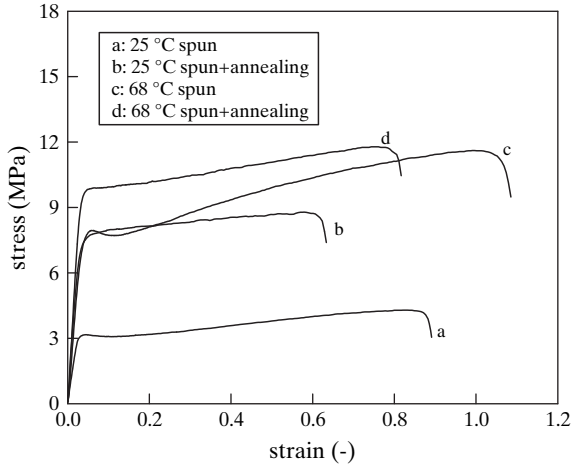

Fig. 11. Stress-strain curves of PDLLA membranes electrospun at different temperatures without and with annealing at 91 °C for 5 min.

route to crossover the binodal curve and enhance the phase separation phenomena. Recently, Dayal et al. [40], have provided the theoretical calculation evidence on the basis of fluid dynamics coupled with the Cahn-Hilliard time evolution equation for phase separation to reveal the possible micro-domain morphology in the electrospinning process. Intuitively, the formation, growth, and deformation of the phase-separated domains in the electrospinning jet eventually affect the final orientation of PDLLA chains developed in the as-spun fiber. Thus, the absence of a specific chain orientation in the electrospun PDLLA fibers was mainly attributed to the phase separation process happening during electrospinning. Using the electron diffraction and WAXD techniques, Dersch et al. [41] have demonstrated that the internal structure of electrospun PLA fibers exhibited no orientational order, and proposed the presence of the phase separation behavior. As shown in Fig. 8, the low and high melting endotherms could be attributed to the melting of PDLLA crystallites in the solvent-rich and solvent-leach domains, respectively, which are developed during the DSC heating scan. This unique morphology of the as-spun fibers implies a new avenue for studying the phase separation phenomena in a micro-sized stretching jet under an extremely rapid solidification, which deserves more attention particularly in controlling the internal structure of the electrospun fibers.

The annealing effect on the fiber morphology is shown in Fig. 10, where PDLLA fibers are apparently fused and connected to each other after the 91 °C annealing. By means of fiber-surface softening and fusion, it seems that short-time annealing at temperatures higher than T_g but lower than the cold crystallization temperature, provides a practical means to enhance the membrane integrity [42]. This is achieved through the increase in crystallinity, as well as the formation of the fiber network. As evidenced by the stress-strain curves in Fig. 11, the Young's modulus and the tensile strength of electrospun membranes are improved by thermal annealing. The determined Young's modulus (E), tensile strength (σ_{max}), elongation at break (ε_{max}) and porosity are displayed in Table 4. Annealing also leads to a slight reduction of the porosity and ε_{max}. It is of interest to note that PDLLA fiber membrane electrospun from the 68 °C solution possesses a larger Young's modulus and a higher tensile strength, compared to the one obtained by room-temperature electrospinning process. Based on the previous results that the Young's modulus of individual nanofibers was increased with decreasing fiber diameter [43], the present mechanical enhancement is attributable to the fine fiber diameter (Table 3) and slightly low porosity (Table 4) of membranes obtained by the high-temperature electrospinning process.

Table 4
Mechanical properties of PDLLA fiber membranes prepared from different processes of electrospinning and thermal annealing.

Membrane	E (MPa)	σ_{max} (MPa)	ε_{max} (−)	Porosity (%)
25 °C spun	125 ± 14	4.3 ± 0.2	0.80 ± 0.16	65
25 °C spun & annealing[a]	242 ± 21	8.8 ± 0.4	0.70 ± 0.10	62
68 °C spun	230 ± 21	10.2 ± 0.8	1.00 ± 0.09	62
68 °C spun & annealing[a]	368 ± 30	11.8 ± 0.2	0.77 ± 0.05	56

[a] Electrospun membranes annealed at 91 °C for 5 min.

4. Conclusion

The diameter of electrospun fiber was found to vary with the zero shear viscosity to the 0.45 power for the PDLLA material. By tuning the operation temperature, solution viscosity was adjusted to a different level, giving rise to a feasible route for manipulating the as-spun fiber diameter. For instance, fiber diameter was dramatically decreased from 503 to 318 nm as the temperature of the electrospinning solution was raised from 25 to 45 °C. Among the three variables available, flow-rate was the dominant electrospinning factor, and the tip-to-collect distance showed no significant effect on the process. For a given solution, a simple relation was obtained: $d_f \sim d_j^{0.61}$ regardless of the processing variables used. Short-time annealing of the nonwoven fabrics led to a rapid crystallization of the phase-separated structure preserved in the electrospun PDLLA fibers, and developed a more integrated network for enhanced mechanical properties.

Acknowledgments

The financial support for this work has been received from the National Science Council of Taiwan (NSC 92-2216-E-006-016), Taiwan Textile Research Institute (TTRI), Industrial Technology Research Institute (ITRI) as well as the NCKU through the "Landmark Program of the NCKU top University Project".

Appendix. Determination of M_e value for PDLLA with L/D = 9/1

We carried out the frequency sweep measurements of the undiluted PDLLA melt at various temperatures (80–210 °C). Based on the time–temperature superposition principle, the master curves of storage modulus (G'), loss modulus (G''), and tanδ ($=G''/G'$) at a reference temperature of 200 °C are shown in Fig. A1. Two typical relations are expected for a homogeneous melt in the low frequency regime, i.e. $G' \sim \omega^{2.0}$ and $G'' \sim \omega^{1.0}$, provided that the longest chains are completely relaxed. For our sample tested, the derived exponents in the low frequency region for G' and G'' are 1.96 and 0.97, respectively, indicating that the terminal region is reached. According to the classical theory, the average molecular weight between entanglements, M_e, is inversely proportional to the plateau shear modulusG_N^0, that is,

$$M_e = \rho RT/G_N^o \quad \text{(A1)}$$

where ρ is the density, R is the gas constant, and T is the absolute temperature. Conventionally, three approaches have been developed to determine G_N^0 from the dynamic properties of polymeric melt [44–46]. The first approach is based on the minimum tanδ criterion, that is, the G' value corresponding to the frequency at which tanδ is minimum is taken as G_N^0. On this basis, the tan $\delta - \omega$ plot exhibits a pronounced minimum (Fig. A1), and the determined G_N^0 is 0.747 MPa. For the present study, the sample density is

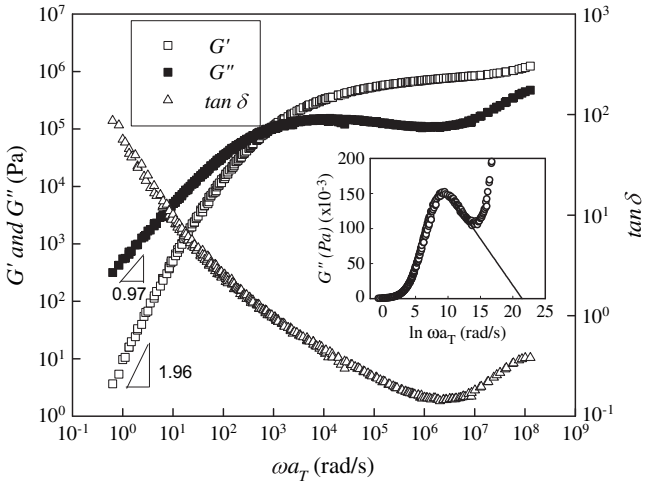

Fig. A1. Master curves of G', G'' and tanδ for PDLLA. The inset shows the plot of G'' versus lnωa_T for obtaining G_N^0 by the integration method.

assumed to be independent of tacticity, and a value of 1.09 g/cm^3 at 200 °C is estimated from the PLLA result [47]. Thus, the derived value of M_e is 5740 g/mol. The second approach is based on the integration method; the plot of G'' versus the natural logarithm of the angular frequency shows a pronounced maximum, and the area under the curve is related to G_N^0 by the following expression:

$$G_N^o = \frac{2}{\pi}\int_{-\infty}^{+\infty} G''(\varpi)d\ \ln\ \varpi a_T \qquad \text{(A2)}$$

The inset in Fig. A1 shows the plot of G'' versus lnωa_T curve, where an evident maximum is observed and a linear extrapolation of G'' curve is reasonably performed to the high frequency regime. The value of G_N^0 derived by Eq. (A2) is 0.766 MPa, which corresponds to a M_e value of 5600 g/mol. The third approach for determining G_N^0 is base on an empirical equation expressed by the following [44]:

$$\log\left(\frac{G_N^o}{G_c}\right) = 0.380 + \frac{2.63\log p}{1 + 2.45\log p} \qquad \text{(A3)}$$

where G_c is the cross-over modulus at which the G' and G'' curves intersect, that is $G'(\omega) = G''(\omega) = G_c$. Eq. (A3) has been derived from a collection of 30 different polymers and has been widely applied for some condensation polymer with limited molecular weight or some crystalline polymers with a narrow temperature window for rheological measurements. It should be noted that Eq. (A3) is only valid provided that the polydisperisty (p) of polymers is lower than 3.0 [44]. For our PDLLA, p is 2.1 obtained from the GPC result, G_c is 0.106 MPa from Figure A1, and a G_N^0 value of 0.754 MPa is determined by Eq. (A3), yielding a M_e value of 5690 g/mol. The M_e determined from the integration method, which is more appropriate and reliable, is slightly smaller than that obtained from the minimum tanδ criterion as well as the empirical equation, and a relative error of ca. 2.5% is found. However, a low M_e of 4000 g/mol at 180 °C has been reported by Dorgan et al. using the integration method [48]. In fact, a wide range of M_e was reported for the PLA: 8000 g/mol at 200 °C [47], 7700 g/mol at 100 °C [49], and 10,000 g/mol obtained by C_∞ [50]). The discrepancy could be attributed to the variation of the chain configuration, i.e. isotactic sequence length, introduced by the difference in the D-/L-form content. The effect of chain configuration on the M_e is currently under investigation in this laboratory.

References

[1] Greiner A, Wendorff JH. Angew Chem Int Ed 2007;46:5670.
[2] Ramakrishna S, Kazutoshi F, Teo WE, Lim TC, Ma Z. An introduction to nanofibers. Singapore: World Scientific Co., Pte. Ltd; 2005.
[3] Reneker DH, Fong H. Polymeric nanofibers. In: ACS symposium series 918. Washington, DC: American Chemical Society; 2006.
[4] Reneker DH, Yarin AL, Zussman E, Xu H. In: Aref H, Van Der Giessen E, editors. Advances in applied mechanics, vol. 41. London: Elsevier/Academic Press; 2007. p. 43–195.
[5] Lyons J, Li C, Ko F. Polymer 2004;45:7597.
[6] Zhou H, Green TB, Joo YL. Polymer 2006;47:7497.
[7] McKee MG, Wilkes GL, Colby RH, Long TE. Macromolecules 2004;37:1760.
[8] Shenoy SL, Bates WD, Frisch HL, Wnek GE. Polymer 2005;46:3372.
[9] Wang C, Hsu CH, Lin JH. Macromolecules 2006;39:7662.
[10] Ohkama K, Minato KI, Kumagai G, Hayashi S, Yamamoto H. Biomacromolecules 2006;7:3291.
[11] Lim LT, Auras R, Rubino M. Prog Polym Sci 2008;33:820.
[12] Mooney DJ, Baldwin DF, Suh NP, Vacanti JP, Langer R. Biomaterials 1996;17:1417.
[13] Garlotta DJ. Polym Environ 2001;9:63.
[14] Tsuji H, Ikada Y. Macromol Chem Phys 1996;197:3483.
[15] Kumbar SG, Nukavarapu SP, James R, Nair LS, Laurenin CT. Biomaterials 2008; 29:4100.
[16] Tan SH, Inai R, Kotaki M, Ramakrishna S. Polymer 2005;46:6128.
[17] Agarwal S, Wendorff JH, Greiner A. Polymer 2008;49:5603.
[18] Zong X, Kim K, Fang D, Ran S, Hsiao BS, Chu B. Polymer 2002;43:4403.
[19] Inai R, Kotaki M, Ramakrishna S. Nanotechnology 2005;16:208.
[20] Bognitzki M, Czado W, Frese T, Schaper A, Hellwig M, Steinhart M, et al. Adv Mater 2001;13:70.
[21] Kim K, Yu M, Zong X, Chiu J, Fang D, Seo YS, et al. Biomaterials 2003;24:4977.
[22] Ishii D, Ying TH, Mahara A, Murakami S, Yamaoka T, Lee W, et al. Biomacromolecules 2009;10:237.
[23] Ogata N, Yamaguchi S, Shimada N, Lu G, Iwata T, Nakane K, et al. J Appl Polym Sci 2007;104:1640.
[24] Legrand P, Lesieur S, Bochot A, Gref R, Raatjes W, Barratt G, et al. Int J Pharm 2007;344:33.
[25] Graessley WW. Viscoelastic and flow in polymeric fluids in physical properties of polymers. Cambridge, UK. 3rd ed.; 2004.
[26] Wang C, Chien HS, Hsu CH, Wang YC, Wang CT, Lu HA. Macromolecules 2007;40:7973.
[27] Wang C, Hsu CH, Hwang IH. Polymer 2008;49:4188.
[28] Zong X, Ran S, Kim KS, Fang D, Hsiao BS, Chu B. Biomacromolecules 2003;4: 416.
[29] Gupta P, Elkins C, Long TE, Wilkes GL. Polymer 2005;46:4799.
[30] Hohman MM, Shin M, Rutledge G, Brenner MP. Phys Fluids 2001;13:2221.
[31] Yarin AL, Koombhongse S, Reneker DH. J Appl Phys 2001;89:3018.
[32] Feng JJ. Phys Fluids 2002;14:3912.
[33] Helgeson M, Grammatikos KN, Deitzel JM, Wagner NJ. Polymer 2008;49:2924.
[34] Meaurio E, Zuza E, López-Rodriguez N, Sarasua JR. J Phys Chem B 2006;110: 5790.
[35] Park JW, Tanaka T, Doi Y, Iwata T. Macromol Biosci 2005;5:840.
[36] Takasaki M, Ito H, Kikutani T. J Macromol Sci Phys B 2003;42:57.
[37] Hoogsteen W, Postema AR, Pennings AJ, ten Brinke G, Zugenmaier P. Macromolecules 1990;23:634.
[38] Aou K, Kang S, Hsu SL. Macromolecules 2005;38:7730.
[39] Megelski S, Stephens JS, Tassi NG, Chase DB, Rabolt JF. Macromolecules 2002;35:8456.
[40] Dayal P, Liu J, Kumar S, Kyu T. Macromolecules 2007;40:7689.
[41] Dersch R, Liu T, Schaper AK, Greiner A, Wendorff JH. J Polym Sci Polym Chem 2003;41:545.
[42] You Y, Lee SW, Lee SJ, Park WH. Mater Lett 2006;60:1331.
[43] Tan EPS, Lim CT. Nanotechnology 2006;17:2649.
[44] Wu S. J Poly Sci Polym Phys 1989;27:723.
[45] Eckstein A, Suhm J, Friedrich C, Maier RD, Sassmannchausen J, Bochmann M, et al. Macromolecules 1998;31:1335.
[46] Ferry JD. Viscoelastic properties of polymers. 3rd ed. New York: John Wiley & Sons; 1980.
[47] Cooper-White JJ, Mackay ME. J Polym Sci Polym Phys 1999;37:1803.
[48] Dorgan JR, Janzen J, Clayton MP, Hait SB, Knauss DM. J Rheol 2005;49:607.
[49] Ren J, Urakawa O, Adachi K. Macromolecules 2003;36:210.
[50] Grijpma DW, Penning JP, Pennings A. J Colloid Polym Sci 1994;272:1068.